Available online at www.sciencedirect.com
ScienceDirect
Geochimica et Cosmochimica Acta 71 (2007) 543–555
Geochimica
www.elsevier.com/locate/gca

Electron tunneling properties of outer-membrane decaheme cytochromes from *Shewanella oneidensis*

Nicholas S. Wigginton [a,*], Kevin M. Rosso [b], Brian H. Lower [b], Liang Shi [c], Michael F. Hochella Jr. [a]

[a] *Center for NanoBioEarth, Department of Geosciences, Virginia Tech, 4044 Derring Hall, Blacksburg, VA 24061, USA*
[b] *W. R. Wiley Environmental Molecular Sciences Laboratory and Chemical Sciences Division, Pacific Northwest National Laboratory, Richland, WA 99352, USA*
[c] *Biological Sciences Division, Pacific Northwest National Laboratory, Richland, WA 99352, USA*

Received 22 May 2006; accepted in revised form 4 October 2006

Abstract

We have characterized the outer-membrane decaheme cytochromes OmcA and MtrC from *Shewanella oneidensis* MR-1 at the single-molecule level using scanning tunneling microscopy (STM) and tunneling spectroscopy (TS). These cytochrome proteins are of great interest because they are thought to mediate bacterial electron transfer reactions in anoxic waters that control the reductive dissolution of oxide minerals. In our study, to characterize the electron transfer properties of these proteins on a model surface, the purified cytochromes were chemically immobilized as molecular monolayers on Au(111) substrates via a recombinant tetra-cysteine sequence as verified by X-ray photoelectron spectroscopy. Atomic force microscopy images confirm the monolayer films were ~5–8 nm thick which is consistent with the apparent lateral dimensions of individual cytochrome molecules obtained with STM. Current–voltage TS of single cytochrome molecules revealed that OmcA and MtrC have different abilities to mediate tunneling current despite having otherwise very similar molecular and biochemical properties. These observations suggest that, based on their electron tunneling properties, the two cytochromes could have specific roles during bacterial metal reduction. Additionally, this study establishes single-molecule STM/TS as an effective means for revealing insights into biogeochemical redox processes in the environment.

1. Introduction

Since life's inception on the planet, microorganisms have been interacting with Earth materials and influencing global geochemical processes (see reviews by Nealson and Stahl, 1997; Newman and Banfield, 2002). In fact, dissimilatory metal-reducing bacteria (DMRB) are thought to be similar to some of the first organisms that evolved on Earth, and hence may represent the first true biogeochemical agents to have existed on our planet (Vargas et al., 1998). Geomicrobiological cycling of metals like iron, the most abundant redox-active metal in the Earth's crust, and manganese by DMRB continues to be a prevalent redox process in modern environments and influences the fate and transport of not only these metals, but of organic and inorganic contaminants as well (Nealson et al., 2002; Lovley et al., 2004; Kappler and Straub, 2005). Given the low solubility, and hence solid-phase, of Fe(III) and Mn(IV) in natural waters, the molecular and nanoscale interactions between oxide surfaces and microorganisms (see reviews by Hochella, 2002; Gilbert and Banfield, 2005) become significant controls on this ubiquitous and dynamic redox couple.

One specific DMRB under widespread study is *Shewanella oneidensis* MR-1, a gram-negative facultative anaerobe that inhabits a wide variety of marine and surface waters as well as soils and sediments in the subsurface critical zone (Myers and Nealson, 1988; Venkateswaran et al., 1999). Recent studies have provided a glimpse into the

* Corresponding author. Fax: +1 540 231 3386.
E-mail address: wigginto@vt.edu (N.S. Wigginton).

0016-7037/$ - see front matter © 2006 Elsevier Inc. All rights reserved.
doi:10.1016/j.gca.2006.10.002

remarkable electron transport chain of *S. oneidensis*, noting the importance of abundant multiheme cytochromes—particularly OmcA and MtrC—in bacterial iron and manganese respiration (see reviews by Tiedje, 2002; Schroder et al., 2003; Dichristina et al., 2005).

OmcA (SO1779) and MtrC (SO1778; also referred to as OmcB) are decaheme *c*-type cytochromes with calculated molecular weights of 83 and 79 kDa, respectively (Myers and Myers, 1997, 1998; Beliaev et al., 2001). Each contains lipoprotein consensus sequences for anchoring to the bacterial outer-membrane (Myers and Myers, 2004). It has been suggested that they have overlapping roles in Mn(IV)-oxide reduction implying that they could both act as terminal metal-reducing enzymes (Myers and Myers, 2003). Further support of this notion has been verified by the demonstration that purified OmcA and MtrC form a stable protein complex that has a higher reduction activity relative to either of the cytochromes alone (Shi et al., 2006). Moreover, the midpoint potentials of OmcA and MtrC have been estimated with electrochemical redox titrations (Richardson et al., personal communication) and suggest that the complex may be tuned to a high redox potential. Despite having a broad biochemical and electrochemical knowledge of the function of these cytochromes, the molecular-scale properties controlling the electron transfer behavior of these cytochromes, particularly in an adsorbed state, remain poorly understood. Moreover, the mechanism(s) by which DMRB utilize these cytochromes to shuttle electrons to iron and manganese-bearing mineral surfaces remains elusive.

One hypothesis under investigation is that the terminal reduction pathway is mediated enzymatically by outer-membrane multiheme cytochromes (e.g., OmcA, MtrC) that are in direct contact with the oxide surface. Evidence supporting this hypothesis has been provided by studies of cell adhesion and direct electron transfer. For example, nanoscale adhesive forces between *S. oneidensis* and goethite (α-FeOOH) may be due to bonding interactions with outer-membrane multiheme cytochromes exposed at the cell surface (Lower et al., 2001, 2005). It has also been proposed that *S. oneidensis* has the ability to distinguish between polyvalent and unreactive metal-oxide surfaces (Lower et al., 2001) and even between different crystallographic faces on one iron-oxide mineral (Neal et al., 2005). Adhesion propensity corresponds quite well to the calculated electron transfer behavior and reactivity at these same faces (Neal et al., 2003), supporting the possibility that interfacial electron transfer and cytochrome-mediated adhesion may be directly related to metal reduction. Presumably this direct contact is necessary to increase the electronic coupling of the cell's electron transfer moieties (e.g., redox-active heme cofactors within membrane-associated cytochromes) to the iron oxide surface allowing for efficient electron transfer (i.e., *tunneling*).

Alternatively, there appears to be substantial evidence supporting indirect reduction pathways that do not require direct contact between the cell and the oxide surface. In these cases, reduction is thought to be mediated either by small redox-active molecules acting as electron shuttles or by the production of extracellular pillin-like appendages recently termed 'nanowires'. In the case of shuttles, it is possible that outer-membrane cytochromes donate electrons to biosynthetic shuttle molecules such as quinones, which then transfer electrons to specific sites on the oxide surface (Newman and Kolter, 2000; Lies et al., 2005). Reduction of hematite (α-Fe_2O_3) surfaces by hydroquinone molecules appears to be a relatively facile process (Stack et al., 2004; Anschutz and Penn, 2005) despite the dramatic influence of adsorption, pH, and quinone structure on the thermodynamics of such reactions (Uchimiya and Stone, 2006). Reductive dissolution features on hematite surfaces observed at locations not associated with specific cell attachment sties of *S. putrefaciens* CN32 (Rosso et al., 2003) may also support this pathway. However, calculated electron transfer rates suggest that the relatively fast diffusion of electrons at hematite surfaces may instead account for non-local dissolution features (Kerisit and Rosso, 2006). Moreover, it has recently been shown that enzyme-containing membrane fractions can directly reduce Fe(III) and Mn(IV)-oxides without the presence of chelators or small electron shuttles (Ruebush et al., 2006).

Secretion of nanowires, so-called because of their apparent ability to conduct an electrical current, was recently proposed to be an alternative pathway for long-range oxide reduction (Reguera et al., 2005; Gorby et al., 2006). Although there are two contradicting reports regarding the nanowires produced by *S. oneidensis*, a recent study shows that not only does *S. oneidensis* produce functional nanowires, but also that its nanowires are composed in part of outer-membrane multiheme cytochromes—the same cytochromes thought to be responsible for direct enzymatic reduction (Gorby et al., 2006).

As is often the case with such dynamic interfaces in microbial systems, the predominating whole-cell mechanism for bacterial metal reduction may in fact be an amalgamation of the three proposed pathways above and may even involve presently unknown mechanisms. Nonetheless, a common component of all direct and indirect solid-phase oxide reduction models is the involvement of outer-membrane multiheme cytochromes, particularly the cytochromes OmcA and MtrC. In this study, we attempt to address an important aspect of the direct enzymatic reduction model by interrogating the ability of OmcA and MtrC to mediate interfacial tunneling current when adsorbed to a solid surface.

To address the need of an analytical technique capable of probing the electron tunneling properties of adsorbed cytochrome molecules, various scanning probe microscopy techniques have historically been employed. To date, scanning tunneling microscopy (STM) and current-sensing atomic force microscopy (CS-AFM), coupled with tunneling spectroscopy (TS) on immobilized single-center metalloproteins, have revealed the nature of interfacial tunneling at a single-molecule level (see reviews by Davis

and Hill, 2002; Zhang et al., 2002; Davis et al., 2005). The development of these techniques has arrived to the point where single-molecule measurements on multicenter metalloproteins are achievable. Here, we have employed these techniques to study the decaheme cytochromes OmcA and MtrC adsorbed to Au(111) substrates with the objective of attempting to directly probe their mechanisms of electron transfer (see Section 2.1 for justification).

In this study, we: (1) establish a protocol for chemical immobilization of OmcA and MtrC in the form of monolayer films on Au(111) surfaces, (2) characterize these cytochrome films using STM, AFM, and XPS, and (3) demonstrate, through current–voltage TS, clear differences in the molecular conductance of the two cytochromes. These tunneling differences may eventually be representative of their intrinsic interfacial electron transfer properties.

2. Materials and methods

2.1. Cytochrome purification and film preparation

The most common substrate used for making single-molecule STM measurements on adsorbed metalloproteins is Au(111). This substrate provides several advantages over oxide surfaces. Au(111) is a stable surface in air and water on the time scale of STM measurements and will not spontaneously oxidize these cytochromes as an iron oxide surface could (e.g., hematite). When properly prepared, an Au(111) substrate is comprised primarily of large atomically flat terraces hundreds of nanometers wide suitable for high-resolution imaging of cytochrome monolayers. Au(111) is an excellent conducting substrate for STM compared to semiconducting oxides. Furthermore, the electronic structure near the Fermi energy for a metal is in general comparatively simple and better understood relative to metal oxides. For example, relatively few features appear in the TS conductance curves for Au(111), and those that do are very reproducible and well understood (Davis et al., 1991; Avouris et al., 1995; Kowalczyk et al., 2006) whereas the same cannot be said for oxide surfaces such as hematite (e.g., Becker et al., 1996). We viewed these Au(111) characteristics to be important for maximizing our ability to interpret the TS data.

The use of Au(111) substrates also provides a key feature in that methods for chemical immobilization of proteins on the surface are already well established. Cysteine residues exposed on many metalloprotein surfaces are able to form covalent thiol bonds with Au(111) which stabilize cytochrome films for imaging with STM. Chemical binding employing a thiol-gold bridge improves chances for efficient electronic coupling between the metalloprotein and the electrode surface (Vondrak et al., 1999). Proteins, and in particular, cytochromes, have been documented to have electrostatic affinities for oxide surfaces (Khare et al., 2005; Eggleston et al., 2006) but protocols for immobilizing cytochromes using chemical binding to oxide surfaces are not well developed at this time. Historically, recombinant proteins with surface-exposed cysteine residues have been constructed to achieve chemical binding (Lo et al., 1999; Andolfi et al., 2002), and that is the strategy used in this study. X-ray photoelectron spectroscopy (XPS) has widely been used to detect such Au–S thiol bonds in organo-sulfur films including single-center metalloproteins (e.g., Chi et al., 2000; Hansen et al., 2003).

Recombinant OmcA and MtrC contained a 4 × Cys/V5/6 × His tag (AACCPGCCKGKPIPQPLLGLDSTRTGHHHHHH) at their C-termini for efficient protein detection, purification, and attachment to the Au(111) surface. The recombinant proteins were expressed in *S. oneidensis*. OmcA was purified as described in a previously established protocol (Shi et al., 2005, 2006) and STM imaging showed OmcA was well bound to the Au surface (see Section 3 for further explanation). In contrast to OmcA, initial STM images of our previously purified MtrC suggested that it failed to bind to Au(111). Because this MtrC was also refractory to the purification by immobilized metal ion chromatography (IMAC) despite the presence of 6 × His tag at its C-terminus, we believed its tag was buried inside the protein molecule. To make its tag surface-exposed, we added a linker sequence (DDDDK) between MtrC and the tetra-cysteine sequence. The newly constructed MtrC bonded well to the Ni-NTA column and was purified by IMAC. Indeed, the newly purified MtrC was firmly bound to the Au(111) surface, and formed a stable film.

The purified cytochromes were stored at −20 °C in buffer solution with the following solutes: 20 mM HEPES, 5 mM β-mercaptoethanol, protease inhibitor, 250 mM NaCl, 1% octyl β-D-glucopyranoside (OGP), and 10% glycerol at pH 7.6. Additional 2 mM β-mercaptoethanol was added to eliminate the formation of disulfide bonds between thiol groups in the tetra-cysteine tag before depositing onto the gold substrate. Due to the presence of lipoprotein consensus sequences for anchoring to the outer-membrane, solubilization in water of the isolated cytochromes requires detergent (OGP) to saturate the exposed hydrophobic regions of the protein surface. The original buffer solution was exchanged twice with 20 mM OGP detergent, 50 mM HEPES buffer, pH 7.6, using Microcon centrifuge filters (10,000 MWCO) at 14,000 rpm and 10 °C (Davis et al., 2000). The concentration of OGP was kept below its critical micelle concentration of 25 mM.

The Au(111) layer was ~200 nm thick, supported on muscovite mica, and freshly annealed in a hydrogen flame (Molecular Imaging, Inc.). A hydrophobic seal was made at the contact between gold and mica using Tempfix adhesive (SPI Inc.) to ensure the protein solution did not contact disrupt the Au(111) surface from underneath. Statically charged particles were then removed with a Zerostat 3 piezoelectric pistol before finally depositing approximately 50 μL of the protein solution (final concentration <20 mM) onto the Au(111) surface. The solution was left in contact with the Au(111) surface for 12–16 h at 4 °C in a glass Petri dish. Afterwards, the protein solution was carefully removed from one corner of the film using a pipette (an area that was not used for imaging) and the remaining solution wicked away using the edge of a Kimwipe until no evidence of solution on the substrate was visibly present. The film was then left to equilibrate at room temperature and ambient humidity for 1–2 h before STM imaging. Extensive rinsing of the films was not necessary as it interferes with the hydrophobic nature of the OGP overlayer (see Section 3.2.1). Films were used for experiments no longer than 10 days after preparation. Control films of 20 mM OGP detergent and 50 mM HEPES buffer were prepared using the same protocol except without protein in solution. Bare Au(111) control samples were only treated with the piezoelectric pistol prior to imaging.

2.2. STM/TS and AFM operation

Using a Molecular Imaging, Inc. Pico SPM controller and 300S-type scanner, STM and AFM imaging was performed in air at ambient humidity. STM imaging was conducted under constant-current mode using electrochemically etched 80:20 Pt–Ir tips. Images were always obtained by using positive bias voltages (~0.5–1 V) for engaging the tip to the sample surface. In this system, the tip is kept at ground potential while the bias voltage is applied to the substrate thus all bias voltages reported reflect the sample bias relative to the tip. AFM images were collected in contact mode using Pt–Ir coated silicon–nitride cantilevers with a force-constant of 0.3 N/m (MikroMasch Inc.).

During TS operation, the magnitude of the tunneling current (I) passing through an individual protein molecule as the bias voltage (V) is changed can be viewed as carrying information regarding the propensity of the cytochromes to specifically mediate electron tunneling between the STM tip and the Au substrate. For the collection of $I(V)$ spectra, the tip was quickly centered over a chosen cytochrome immediately after its appearance in an STM image. The feedback loop was automatically turned off, and the tunneling current was recorded as a function of applied bias voltage. The bias was swept through a 3 V range from +1.5 to −1.5 V at 10 ms sweep duration. Each spectrum consisted of 200 sampling points. Tunneling spectra were always collected starting from the same imaging bias voltage and set point current. The bias voltage sweep was always in

the same direction. The representative cytochrome $I(V)$ spectra presented below are averages of several thousand individual spectra (3050 for OmcA, ~8000 for MtrC) collected on several different protein films using many different Pt–Ir tips. Raw $I(V)$ spectra were initially analyzed using Igor Pro 4.0 (Wavemetrics, Inc). Extreme outliers with obvious differences in $I(V)$ signal (<5%) were removed before the remaining spectra were averaged together to construct the representative spectra presented below. Differential conductance (dI/dV) spectra were generated using the Savitzky and Golay (1964) moving least-squares method and a 23-point window and removing discontinuities at zero bias voltage. Normalized differential conductance spectra [$(dI/dV)/(I/V)$] were generated by normalizing to the best-fit exponential 'background'.

All spectra were collected at an initial tip–sample separation distance as defined by 1.08 V and 0.5 nA. Additionally, in every case the collection of each $I(V)$ curve as described above was automatically repeated at five different increasing tip–sample distances (Z) in 1 Å steps from the original separation distance. This allowed for analysis of $I(Z)$ spectra for chosen bias voltages. Exponential decay in the $I(Z)$ spectra was used as a check to ensure that true tunneling was always occurring during the measurements (i.e., currents were attributed to electronic tunneling as opposed to electrochemical or ionic charging).

2.3. XPS operation

All XPS spectra were obtained with a Perkin-Elmer 5400 X-ray photoelectron spectrometer (Physical Electronic Industries, Inc.) using an aluminum X-ray source and two-channel collector. The X-ray anode was operated at 12 keV and 250 W and the vacuum was kept below 5×1^{-7} Torr. The pass energy for wide-range survey scans was 89.45 eV, and for narrow scans it was 17.9 eV. The S 2p spectra presented are averages of 100 sweeps from 178 to 158 eV binding energy with 25 ms for every 0.1 eV step. All spectra are referenced to Au $4f_{7/2}$ at 83.8 eV. Data was analyzed using AugerScan 3.12 (RBD Enterprises Inc.).

3. Results and discussion

3.1. X-ray photoelectron spectroscopy

Survey XPS scans of OmcA and MtrC films, as well as a control film comprised of only OGP detergent and HEPES buffer, show the presence of several Au photopeaks, as well as C 1s, N 1s, and O 1s photopeaks. The absence of a Fe $2p_{3/2}$ photopeak indicated that heme Fe atoms in the cytochromes were below XPS detection limits. Despite a low signal-to-noise ratio, measurable differences were apparent in the narrow scans of S 2p photopeaks between 178 and 158 eV binding energies for OmcA and MtrC films and the OGP control film (Fig. 1). Although its intensity is weak, the representative peak near 162–162.7 eV observed in OmcA and MtrC samples is indicative of thiol bonds with Au(111) (Chi et al., 2000; Duwez, 2004). This peak is absent in the OGP control film, suggesting that the objective of creating a thiol bond between the cytochrome films and the Au substrate was achieved.

We also observed the presence of an additional weak S 2p peak near 168.5 eV in both cytochrome samples. In other organo-sulfur self-assembled monolayers (SAMs), a primary cause of weak unexpected higher energy peaks is oxidation of the sulfur species on a time scale of less than 4 h for films exposed to air (Schoenfisch and Pemberton, 1998). Although the additional peak is not indicative of any chemical interaction with the Au(111) surface, its presence suggests that not all sulfur in the film is associated with Au–S bonds. This is not surprising as there are unbound sulfur species associated with β-mercaptoethanol and HEPES buffer, as well as non-binding cysteine residues in the cytochromes. However, in organo-sulfur SAMs, unbound thiols are expected to have peaks slightly above 163 eV (Duwez, 2004); no such peaks were detected. Due to the relatively low sulfur content in these cytochrome films, it is not unexpected to see weak S 2p photopeaks. If oxidation is indeed occurring on the films, it may also be contributing to the loss of intensity arising from thiol sulfur species.

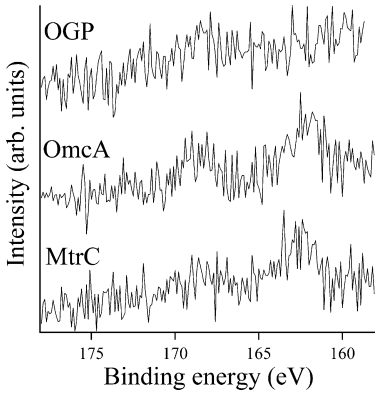

Fig. 1. XPS spectra in the S 2p region for OGP, OmcA, and MtrC samples on Au(111) substrates. Pass energy, 17.9 eV.

These measurements only qualitatively suggest the presence of such interactions between the tetra-cysteine tag and Au(111). They do not suggest all of the molecules are bound in this fashion nor does it eliminate the possibility of other unreacted thiols present in the film. Nevertheless, when the XPS evidence for the presence of thiol bonds is combined with the STM observations below, immobilization of the cytochromes into stable films is clearly established. Note also that the presence of Au–S bond implies minimal separation between the cytochrome molecule and the Au(111) surface, increasing the probability for electronic interactions between one or more redox-active heme cofactors and the gold surface.

3.2. STM/AFM observations

3.2.1. Initial STM imaging

We first characterized freshly annealed clean Au(111) surfaces with STM in ambient conditions at a variety of imaging length scales. The observed topographic features consisted of large terraces separated by monoatomic steps, as expected for this well-studied surface (e.g., Han et al., 1997; Zhang et al., 2004; Morimoto et al., 2005). For the cytochrome films, while the general 'terraced' structure of the underlying Au(111) surface was still evident (see Fig. 2A), high-resolution images of the terraces showed strikingly different features on the terraces themselves. Based on other studies of STM imaging of metalloproteins

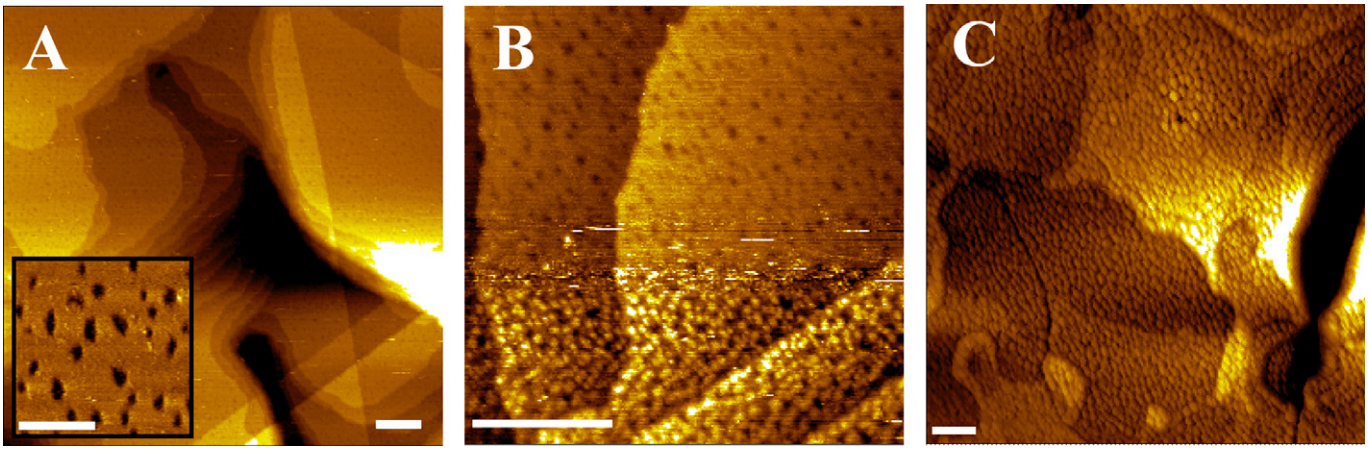

Fig. 2. Series of typical STM topographs of 'unactivated' topography (A), a single irreversible 'activation' event (B), and 'activated' topography of cytochrome films (C). Bias voltage for A was 0.84 V. For B, the bias voltage was lowered from 1.08 V (top of the image) through zero bias until finally stopping near −1.5 V where the abrupt change in image contrast occurs. The bias voltage was then raised through zero bias back to +1.08 V. Bias voltage for C was +2.2 V. 0.5 nA current set-point for all images. Scale bars are 50 nm for A–C and 20 nm for the inset in A.

and the molecular weights of OmcA and MtrC, we expect that individual protein molecules should appear as 'bumps' on the order of a few nanometers in diameter (e.g., Friis et al., 1999; Chi et al., 2000, 2001; Davis and Hill, 2002; Andolfi et al., 2003; Bonanni et al., 2003; Hansen et al., 2003; Andolfi et al., 2004b; Zhang et al., 2004). No such features were initially observed. Instead, images initially consisted of large flat terraces each covered with randomly dispersed patches, or 'pits', of low apparent tunneling probability.

The 'pits' were ~1–3 nm wide and irregularly spaced (Fig. 2A, inset), with an STM apparent depth of ~2–3 Å. Features similar to these have been reported in the literature for other systems, primarily for organo-sulfur self-assembled monolayers (SAMs) (see reviews by Poirier, 1997; Yang and Liu, 2003; Vericat et al., 2005). 'Pits' have also been observed in ambient conditions on alkanethiol-functionalized Au(111) substrates with adsorbed metalloprotein monolayers (e.g., Chi et al., 2000, 2001; Zhang et al., 2003a,b, 2004). In our experiments, images such as these were routinely obtained initially from film to film regardless of cytochrome type. These image features were stable for indefinite periods of time. Imaging at very small length scales did not resolve any features that could assigned as individual cytochromes. For reasons discussed below, we will refer to this initial SAM-like topography as the 'unactivated' film topography.

3.2.2. 'Activation' of cytochrome films

Despite this apparent failure to resolve individual cytochromes initially, we discovered that the cytochromes were indeed present, residing as an intact monolayer that could only be resolved by STM after modifying the tunneling conditions. Here, we describe this process in detail.

By varying the bias voltage to increasingly more negative values, the SAM-like features on the Au(111) terraces could be immediately changed. Bias voltages more negative than ~−1.5 V led to the appearance of clearly resolved features consistent with a monolayer of cytochromes. The resulting images, collected after having surpassed the threshold bias voltage, are referred to as the 'activated' film topography. The transition between 'unactivated' and 'activated' film topographies was very rapid, often shorter than the time required to collect a single scan line, yielding a very sharp transition in the images (Fig. 2B). The images after activation showed a layer of close-packed, nearly spherical features ranging from 5 to 10 nm in size, consistent with the expected sizes for OmcA and MtrC (Fig. 2C). These features uniformly covered entire Au(111) terraces and did not show any preferential adsorption to specific topographic features on the surface. Step heights consistent with those of the underlying Au(111) surface were maintained. Imaging conditions were stable and data could be collected for hours at variable bias voltages even outside the normal bias range of ±1.5 V. The new features assigned as cytochromes are acquired at the expense of the old SAM-like features in an irreversible fashion. For instance, following film activation at large negative bias voltages, the apparent 'pits' were irretrievable upon readjusting the bias voltage back to the low positive values used for engaging the tip to the sample.

Several lines of evidence lead us to conclude that this activation behavior arises due to bias-induced interactions between the tip and a SAM-like overlayer of residual OGP detergent 'blanketing' the cytochrome film. The nominal interpretations of the origin of apparent 'pits' in SAMs are that they arise from either gold substrate vacancy islands that form during the self-assembly process, domain boundaries where the SAM is highly disordered, or molecular defects in the SAM (Vericat et al., 2005). We do not expect gold vacancy islands to contribute to the self-assembled OGP overlayer given the fact that there is a considerably large cytochrome monolayer sandwiched between the gold substrate and OGP. Disorder in the OGP overlayer

may possibly be causing the 'pits', but because of the presence of the underlying cytochrome film it is reasonable to expect that the 'pits' could arise from subtle irregularities in the cytochrome distribution.

Bias-dependent reorganization of self-assembled surfactant films has been previously observed (Boussaad and Tao, 1999). Based on this fact and the observations described above, we rationalize the observed behavior as follows. During deposition and self-assembly of the cytochrome film, as cytochromes bind to the Au(111) via thiol bonds, OGP maintains interaction with the hydrophobic domains of the cytochrome. The hydrophilic polar head group of OGP remains exposed to the aqueous solution while the cytochromes themselves have minimal contact with solution. As the packing of cytochromes approaches a full monolayer and the molecules become densely packed on the surface (see Fig. 4), the OGP facing the solution phase self-assembles into a largely ordered detergent overlayer protecting the hydrophobic cytochromes from solution.

When the bias voltage is assigned a large magnitude at negative bias voltage, the electric field between the tip and sample is evidently strong enough to disrupt the OGP overlayer while not altering the underlying cytochrome film itself. The metal STM tip is strongly hydrophilic and in principle can interact with hydrophilic head groups of the upper surface of the OGP overlayer if enough energy is supplied. We hypothesize that the electric field induced at high bias voltage induces rearrangement of the self-assembled OGP overlayer under the tip so that the outward-facing hydrophilic head groups of OGP wet the tip. This removes intervening detergent from between the tip and cytochrome film, creating a 'window' through the otherwise intact surfactant overlayer allowing the STM tip to engage the underlying cytochrome film directly (Fig. 3). This is what is reflected in the transition from unactivated to activated film topographies in the STM images. Tip wetting phenomena such as this are not uncommon for STM performed in air under ambient conditions (Patel et al., 1997). Further support of this hypothesis is the observation that STM images of activated films could be reverted back to the unactivated film topography only when the tip is fully disengaged from the sample surface. Re-engaging in the same location showed that the OGP overlayer is locally restored and the previously formed 'window' was eliminated. This observation suggests that bias-induced transformation of the tip structure is not responsible for the activation effect. Additional evidence against changes in tip structure include the reproducibility of the observations as well as the stable imaging of the activated cytochrome films over a wide range of bias voltages after activation.

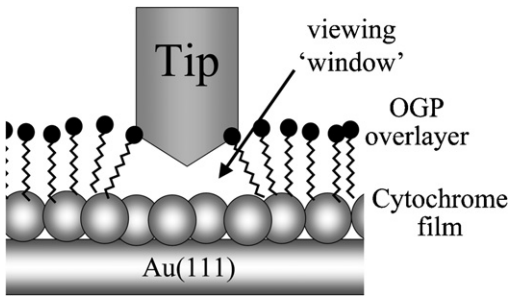

Fig. 3. Cartoon of bias-induced viewing 'window' formed from reorganization of OGP overlayer (film 'activation') revealing an intact cytochrome layer underneath.

The 'window' formed between the tip and OGP overlayer is very stable as long as the tip is engaged, traveling perfectly with the tip during scanning with no signs of interference with imaging. The 'window' is also stable during the collection of $I(V)$ spectra and we found no evidence that the 'window' could be closed by the same electrostatic mechanism by which it is opened, for example by reversal of the bias polarity to large positive values. Therefore, after creation of the activation 'window', the collection of $I(V)$ spectra could involve a wide bias range as needed. In contrast, the collection of $I(V)$ spectra on the unactivated films, i.e., on the SAM-like OGP overlayer were limited to a bias range that did not surpass the threshold bias.

3.2.3. STM of cytochrome molecules

OmcA molecules were observed to be ~8 nm in diameter laterally on average whereas MtrC molecules appeared to be ~5 nm in diameter on average (Fig. 4). The observed sizes of the cytochromes in the activated films are within the expected range for globular proteins of a similar molecular weight, as expected for ambient imaging of biomolecules (Alliata et al., 2004). The apparent sizes observed on the films, including the slight variation between OmcA and MtrC, may be a function of not only their molecular shapes, but whether or not the cytochromes are binding to the Au(111) surface in a preferred orientation.

Because crystal structures for either cytochrome are unavailable, it is unknown, in terms of location on the protein surface and molecular axis, where the cysteine residues that covalently bond to the substrate are exposed. However, there is evidence to indicate binding of both cytochromes to the Au(111) surface is through the tetra-cysteine tag located at the C-termini of the cytochromes. Although recombinant OmcA and MtrC have 27 and 29 cysteines in their polypeptides, respectively, 20 of them are used to covalently bind 10 heme moieties; another serves as the lipid-binding site. Thus, only six and eight cysteine residues are free, respectively, for each polypeptide to bind to Au(111), in which four are from the tetra-cysteine tag. As a control, we attempted to image purified MtrA, a 32 kDa periplasmic (i.e., soluble) decaheme *c*-type cytochrome from *S. oneidensis* (Pitts et al., 2003). Due to the fact that MtrA contains no tetra-cysteine tag, stable films were not observed. Instead it was found that MtrA molecules were easily moved about on the Au(111) surface by the STM tip. Furthermore, MtrC with a recessive tetra-cysteine tag (i.e., the recombinant MtrC that lacks a DDDDK linker sequence between its C-terminus and the tetra-cys-

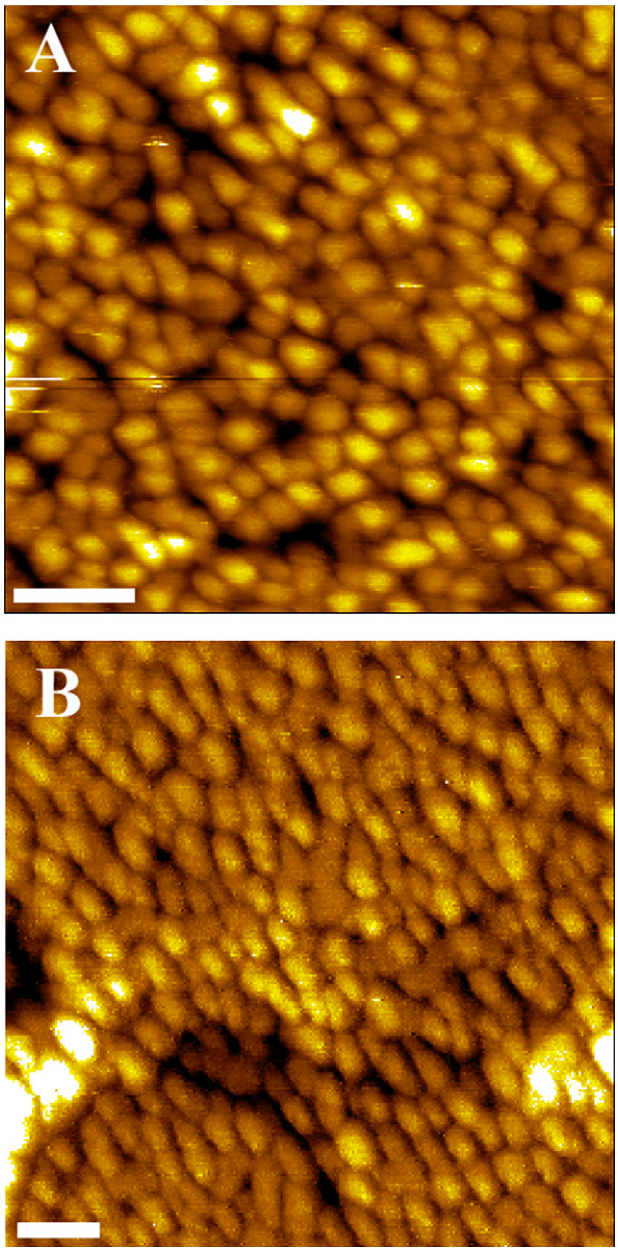

Fig. 4. Typical STM topographs of 'activated' MtrC (A) and OmcA films (B). Tunneling conditions for MtrC: bias voltage 1.08 V, current setpoint 0.5 nA. Tunneling conditions for OmcA: bias 2.2 V, current setpoint 0.5 nA. Scale bars, 20 nm.

teine tag; described in Section 2.1) did not bind to IMAC columns and no images of cytochrome molecules on gold were obtained using STM on this particular MtrC construct. Therefore, there is substantial evidence suggesting an exposed C-terminus tetra-cysteine tag mediates chemical immobilization of OmcA and MtrC on the Au(111) surface.

3.2.4. AFM of cytochrome films

STM does not provide true height information of the adsorbed cytochromes. In an effort to determine the vertical dimensions of individual cytochromes for comparison with the lateral dimensions observed by STM, contact-mode AFM imaging of the cytochrome films was conducted in air and solution. After repeated failed attempts to achieve molecular resolution in solution, the height of the film itself was assessed by imaging in air. Due to capillary and van der Waals forces from imaging in air, we had poor control on the applied forces, which often led to shearing away portions of the cytochrome film from the surface. This however facilitated measurements of the film thickness by comparing the height difference between the upper surface of the film and the underlying Au substrate. The contrast of the intact film to that of the previous scan area is clearly evident (Fig. 5).

The horizontal cross-section in Fig. 5, which bisects the previous scan area indicated by the ~2.7 μm square feature in the center of the image, suggests the cytochrome film thickness is roughly 5–8 nm. This is in excellent agreement with the STM apparent diameters of the cytochromes, and confirms the fact that these films consist of only one monolayer of globular-shaped cytochrome molecules. It should be noted that no activation technique was needed to visualize the films, as expected due to the high loading forces involved with contact mode AFM relative to STM.

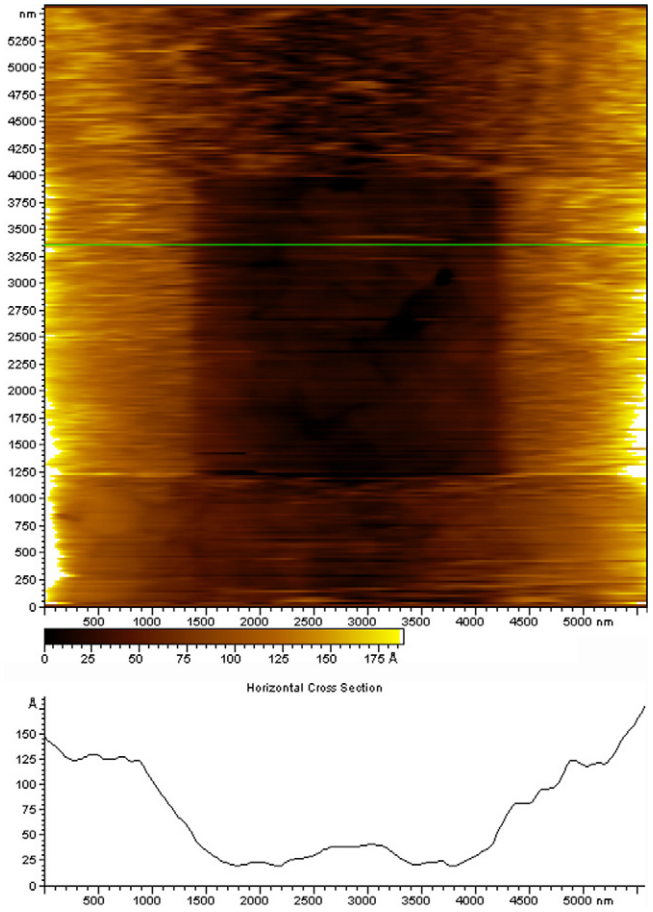

Fig. 5. AFM image of MtrC film showing topographic data with an associated cross-section shown below corresponding to the green line through the center of the image.

3.3. Tunneling spectroscopy

3.3.1. Current–voltage tunneling spectra

TS was used to gain insight into the electron tunneling properties of individual OmcA and MtrC molecules. Representative $I(V)$ spectra for clean Au(111), OmcA, and MtrC are shown in Fig. 6A. As expected, the most obvious difference is between the clean Au(111) and the cytochrome films. Clean Au(111) has a very steep exponential rise in the current with increasing bias voltage magnitude as expected for a metallic substrate, whereas the cytochrome spectra are consistent with a more resistive tunneling junction. The $I(V)$ behavior for OmcA is near exponential, but the $I(V)$ behavior for MtrC is noticeably different in that it does not follow a smooth functional form in the positive bias region. The general features of the $I(V)$ spectra just described are highly reproducible on average for individual cytochromes in these films.

For each TS location, we collected $I(V)$ spectra at five tip–sample separations starting from the imaging tip–sample separation distance and increasing by 1 Å 'Z' increments. The entire spectral set at each sampling location is collected in 50 ms by software automation to minimize the effects of drift. This provided us with the ability to assess the decay in the tunneling current as a function of tip–sample separation for any bias voltage in the $I(V)$ range. $I(Z)$ spectra were used to ensure that the current was a true tunneling current as opposed to electrochemical or ion conduction currents. True tunneling current decays exponentially with increased separation whereas ion conduction has a linear $I(V)$ signature (Hamers, 1993). Fig. 6B shows representative spectra for OmcA at selected bias voltages. Exponential dependence on separation distance is demonstrated across the entire bias range. This verifies that the primary contribution to the STM was from true electronic tunneling through the cytochromes.

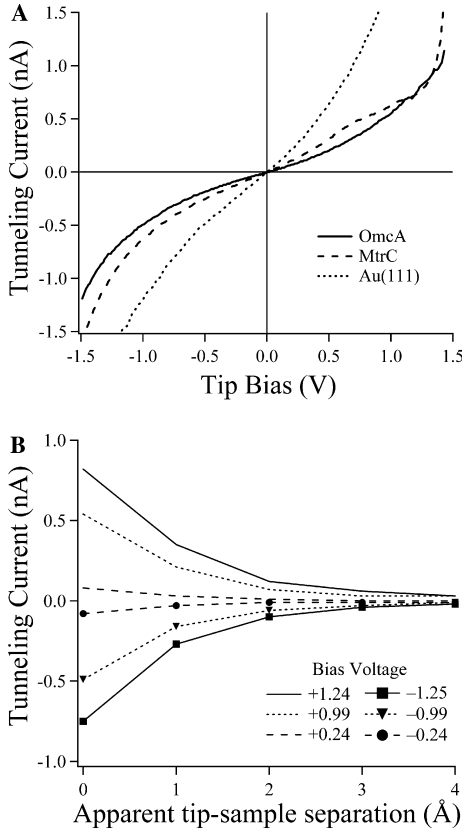

Fig. 6. (A) Representative $I(V)$ spectra on Au(111) and activated cytochrome films of OmcA, and MtrC. Imaging bias voltage, 1.08 V; current set-point, 0.5 nA. (B) Representative $I(Z)$ curves for OmcA and MtrC collected at six different bias voltages, where zero tip–sample separation is defined as the separation distance for imaging at each particular bias voltage and set-point current conditions.

As a check to ensure we were probing only the tunneling properties of the cytochromes and not other molecules possibly in the tunneling junction (e.g., detergent or buffer molecules), $I(V)$ spectra were taken on the OGP overlayer—on unactivated terraces and within the apparent low-tunneling 'pits'—and on the OGP-only film that was described above in Section 2.1. The $I(V)$ spectra on these three surfaces were highly asymmetric with little increase in current in the positive bias range (Fig. 7). This rectifying behavior is a phenomenon that has been observed by STM elsewhere, for example, on copper-phthalocyanine molecules (Pomerantz et al., 1992) as well as on photosynthetic proteins (Stamouli et al., 2004). The $I(V)$ behavior on the unactivated OGP overlayer is very similar to the $I(V)$ behavior of the OGP-only film. The fact that near-symmetric (i.e., non-rectifying) exponential $I(V)$ curves are always observed for OmcA and MtrC (Fig. 6A) but never on the control films suggests that, after activation and the formation of the 'window', the OGP overlayer does not affect the $I(V)$ measurements on the cytochromes.

3.3.2. Normalized differential conductance

Normalized differential conductance spectra (Fig. 8) plotted for OmcA and MtrC enhance the subtle differences in the $I(V)$ spectra. Inflections in slope of the $I(V)$ spectra appear as peaks in the dI/dV form and, when normalized

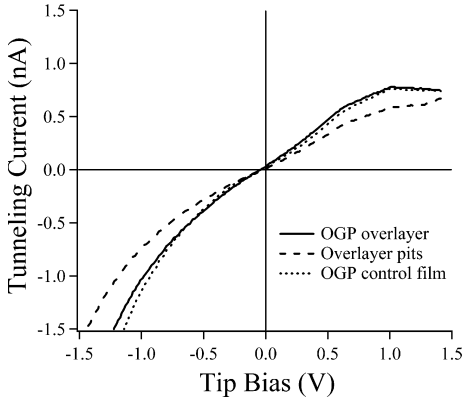

Fig. 7. Representative $I(V)$ spectra of OGP films (dotted) as well as two different locations on the 'unactivated' topography of MtrC cytochrome films; SAM-pits (dashed) and 'unactivated' terraces on the OGP overlayer (solid). Imaging bias voltage, +1.08 V; current set-point, 0.5 nA.

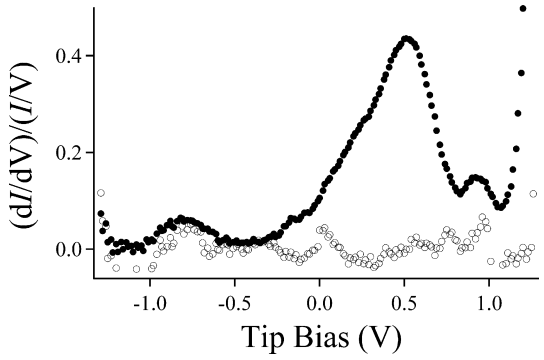

Fig. 8. Normalized differential conductance [(dI/dV)/(I/V)] spectra for OmcA (open circles) and MtrC (closed circles) 'activated' cytochrome films.

to I/V, the bias-dependence of the tunneling transmission probability is removed (Hamers, 1993). This mode of analysis stems from Tersoff–Hamann tunneling theory which provides for the possibility that under ideal conditions at low bias voltage, peaks that appear in the (dI/dV)/(I/V) spectra approximately correspond to a high local density of states of the sample at the location of the tip (Tersoff and Hamann, 1985). Under this assumption, the (dI/dV)/(I/V) spectra for MtrC reflects a large density of states evident in the positive bias range while OmcA shows no such features. This is the first glimpse into the electronic structure of these two redox-active metalloproteins.

Because the representative spectra shown in Fig. 6A for OmcA and MtrC are averages of several thousand individual I(V) spectra, the corresponding peaks in the (dI/dV)/(I/V) spectra may have been slightly broadened. However, based on other STM studies of small redox-active molecules, the effect of averaging still maintains peak positions within $\pm$0.1 V from individual I(V) measurements (Han et al., 1997). The differences seen in the tunneling spectra are thus statistically significant and correspond to true differences in the tunneling conductance of OmcA and MtrC.

If the cytochrome molecule being probed possesses unoccupied or partially occupied energy levels lying between the Fermi levels of the tip and substrate (which are energetically separated by the bias voltage), then in principle these energy levels can assist in the tunneling process (see reviews by Nitzan and Ratner, 2003; McCreery, 2004). Ignoring different possible mechanisms for tunneling current modification due to these 'bridge' states for the moment, in general normalized differential conductance spectra would show increased conductance in the bias voltage range where this condition is met. The assist mechanism is due to either resonant tunneling (Schmickler, 1993), where electrons tunnel directly between tip and substrate by a resonant transition through the unoccupied levels of the molecule, or it is due to "two-step electron transfer" where electrons transferred into the acceptor level are partially stabilized and even temporarily trapped there by nuclear relaxation (Kuznetsov et al., 1992). The difference lies in the energetic position of the bridge state(s) relative to the tip or substrate Fermi levels, the electronic couplings between the tip, molecule, and substrate, and the vibrational dynamics of the molecule. These details are beyond the scope of the current paper. Using electrochemical STM in electrolyte solution under bipotentiostat control, redox energy levels can sometimes be tuned into or out of tunneling resonance, but these experiments are extremely difficult (e.g., Tao, 1996). In our case the measurements are performed without electrochemical control and therefore the cytochrome energy levels sampled during the bias voltage ramp, if any, are by pure chance. It is noteworthy that for these experiments, TS in air provides an advantage over aqueous solution-based TS (e.g., via electrochemical STM) in that the cytochromes used in this study are not expected to be stable over long time scales in solution as they are primarily hydrophobic.

Due to the natural function of these cytochromes for electron transfer—specifically optimized for efficiency without dissipating painstakingly harvested energy—it is natural to consider peaks in the MtrC spectra (Fig. 8) as arising from participation of heme cofactor electronic energy levels in the tunneling process. However, other possible explanations for the observed bias-dependent conductance changes should be considered first. In general, ET rates depend strongly on the dielectric properties of the surrounding medium, with larger reorganization free energies and therefore slower ET rates occurring in polar media with high dielectric constants, such as water (Marcus and Sutin, 1985). In biological ET, a primary function of the protein is to create a low dielectric environment around the heme cofactors to limit the medium contribution to the reorganization free energy. Proteins accomplish this by folding in such a way so as to exclude solvent water from around the heme groups, creating a compact environment with low polarizability. At equilibrium, the structure adopted entails a complex balance between intraprotein, protein–solvent, and solvent–solvent interactions (Simonson, 2003). In multiheme proteins, another primary function of the protein is to facilitate interheme ET, either by arranging heme cofactors in close proximity to each other (usually between 5 and 10 Å apart) or by providing intervening functional groups that can act as electron tunneling bridges, allowing interheme ET distances of up to 14 Å (Page et al., 1999).

We now expand this picture by considering factors relevant to interrogating electron tunneling behavior of a protein using tunneling spectroscopy: (1) Many proteins are charged and have a net permanent dipole in their native conformation (Simonson, 2003). In principle, the charge and/or dipole can couple to the electric field in the tip–sample junction leading to protein orientation or conformation changes with changing bias, particularly when the bias polarity is changed; (2) The structure of the protein is usually coupled in a significant way to the oxidation state of its heme cofactors (Gray and Winkler, 2003). Thus the protein conformation is redox-dependent. This means that variable forces applied to the cytochrome by the changing tip–sub-

strate field could in principle concomitantly shift heme electronic energy levels; and (3) Solvent and ion access to heme or chargeable functional groups in the protein depends on protein structure. By affecting the protein structure, the bias voltage ramp could therefore alter dielectric or protein charge characteristics which in turn would affect the bias-dependence of the tunneling process. To illustrate a possible effect of the large electric fields in the tip–sample junction, it is easy to show that the force on a single test charge in a model tunneling junction under conditions used here are on the nN scale (i.e., bond breaking). For example, the electric field magnitude (E) across a 5 nm tip–substrate tunneling gap filled with protein (dielectric constant $\kappa \sim 10$) (Marcus and Sutin, 1985) is $\sim 3 \times 10^9$ N/C. Assuming the force is proportional to the magnitude of the charge (q), a test charge of 1.6×10^{-19} C would be subjected to ~0.5 nN of force towards the negatively charged electrode. For comparison, previously measured forces attributed to conformational unfolding of outer-membrane proteins in *S. oneidensis* are on the order of 0.2–1 nN (Lower et al., 2001). The effects of multiple charges and/or dipoles in the tunneling gap may induce even stronger net forces acting on the molecule, but such effects are difficult to predict and are considered outside the scope of this paper.

Therefore, despite the numerous recent examples in the literature that have utilized STM on metalloproteins in air as an effective means of single-molecule analysis (e.g., Davis et al., 2000; Chi et al., 2001; Andolfi et al., 2003; Bonanni et al., 2003; Alliata et al., 2004; Andolfi et al., 2004a,b; Davis et al., 2004), there is always a concern regarding effects of the STM measurement itself on the proteins under study. However, it is clear from the high reproducibility of the STM images and TS data in this study that the electric fields associated with STM operation are not irreversibly altering the proteins. Upon film activation, the proteins are very stable under the tip for long periods of repeated scanning and over a wide range of bias voltages. We note also that electric fields of this magnitude are expected to be intrinsically imposed on these kinds of proteins when embedded in a bacterial outer membrane (Lindsay, 1993). In our case, we attribute the stability of the proteins in part to preservation of the local microenvironment (hydration, local saturation of hydrophobic domains, etc.) by the OGP overlayer. Although we cannot claim that the cytochromes are in their native conformation on the surface initially or during STM imaging, reproducible cytochrome dimensions before and after the collection of TS spectra suggest that the molecules are retaining a stable conformation.

Notwithstanding the possible field-induced effects, we conclude in this case that none of them are likely causes for the observed differences between MtrC and OmcA in the normalized differential conductance spectra (Fig. 8). Although the structures of OmcA and MtrC are not yet known, there is substantial evidence suggesting these two proteins are structurally and chemically very similar, beyond the simple fact that they are both decaheme cytochromes with similar molecular weight and size. For example, both MtrC and OmcA are functional Fe(III)-NTA reductases that lack activity toward nitrite or nitrate, with virtually identical rates of Fe(III)-NTA reduction and maximum activity in the same temperature and pH range (Shi et al., 2006). In their oxidized forms, the ferric heme iron ions are low spin species with histidine ligands providing both the distal and proximal ligands in both MtrC and OmcA (Richardson et al., personal communication). Both cytochromes exhibit heme operating potentials within a similar range, with both ranges notably higher than seen for similar proteins from a number of *Shewanella* species. The most significant difference shown so far between MtrC and OmcA is in the 'clustering' of the redox potentials of their 10 heme groups, with MtrC potentials occurring in the region of −80 to −170 mV in a 3:7 ratio and OmcA potentials occurring at −66, −149, and −212 mV in a 3:3:4 ratio (Richardson et al., personal communication). We therefore expect these two proteins to behave similarly within the tunneling junction except for the energy and density of electronic states associated with heme groups. Returning now to the clearly observable differences in the OmcA and MtrC normalized differential conductance spectra (Fig. 8), given the above considerations and given that no structural changes in the cytochromes are evident after collection of tunneling spectra, we conclude that features in the MtrC spectra derive from the participation of heme electronic energy levels in the tunneling process. For OmcA no such features are seen. The tunneling process through OmcA is therefore a so-called 'direct tunneling' mechanism between tip and substrate, wherein the OmcA molecule provides only a smooth modification to the tunneling transmission probability over the bias range used (Fig. 6A). Interpretation of the features observed in the MtrC spectra in terms of a physical model of electron transfer is left to future work.

4. Conclusions

OmcA and MtrC, two decaheme *c*-type cytochromes from *S. oneidensis* proposed to be responsible for direct enzymatic reduction of oxide surfaces have different abilities to mediate interfacial tunneling current when adsorbed to a solid surface. The differences in the tunneling conductance may reflect variation in the roles of these otherwise very similar cytochromes during enzyme-mediated bacterial metal reduction. These results could also have implications for other metal reduction pathways by possibly providing insights into the origin of the conductive properties of bacterial nanowires and/or helping describe extracellular electron transfer interactions between multiheme cytochromes and electron shuttles. How this relates to their electrochemical properties and their operation as a protein complex is yet to be determined. Towards this end, analysis of the tunneling spectra in terms of models based on electron transfer theory may allow for new insights into the mechanisms of elementary electron transfer processes med-

iated by OmcA and MtrC at oxide surfaces. Future experiments employing similar techniques may help constrain the nanoscale redox reactions that occur at the dynamic interface between bacteria, cytochromes, and oxide surfaces.

Acknowledgments

The authors thank Svetlana Yanina for helpful discussions, Frank Cromer for assistance with XPS measurements, and Carrick Eggleston and one anonymous reviewer for thoughtful comments that improved the manuscript. A portion of the research was performed as part of an EMSL Scientific Grand Challenge project at the W. R. Wiley Environmental Molecular Sciences Laboratory, a national scientific user facility sponsored by the DOE Office of Biological and Environmental Research (OBER) and located at Pacific Northwest National Laboratory (PNNL). PNNL is operated for the DOE by Battelle Memorial Institute under Contract DE-AC05-76RL01830. KMR acknowledges the support of the Stanford Environmental Molecular Sciences Institute jointly funded by NSF and DOE OBER; BHL acknowledges the support of the Geosciences Research Program of the DOE Office of Basic Energy Sciences (OBES); LS acknowledges the support of Genomics-Genomes to Life Program of DOE OBER; and MFH acknowledges the support of DOE OBES contracts DE-FG02-02ER15326 and DE-FG02-06ER15786, and NSF contract EAR-0103053.

Associate editor: Carrick M. Eggleston

References

Alliata, D., Andolfi, L., Cannistraro, S., 2004. Tip to substrate distances in STM imaging of biomolecules. *Ultramicroscopy* **101**, 231–240.

Andolfi, L., Cannistraro, S., Canters, G.W., Facci, P., Ficca, A.G., Van Amsterdam, I.M.C., Verbeet, M.P., 2002. A poplar plastocyanin mutant suitable for adsorption onto gold surface via disulfide bridge. *Arch. Biochem. Biophys.* **399**, 81–88.

Andolfi, L., Bonanni, B., Canters, G.W., Verbeet, M.P., Cannistraro, S., 2003. Scanning probe microscopy characterization of gold-chemisorbed poplar plastocyanin mutants. *Surf. Sci.* **530**, 181–194.

Andolfi, L., Bruce, D., Cannistraro, S., Canters, G.W., Davis, J.J., Hill, H.A.O., Crozier, J., Verbeet, M.P., Wrathmell, C.L., Astier, Y., 2004a. The electrochemical characteristics of blue copper protein monolayers on gold. *J. Electroanal. Chem.* **565**, 21–28.

Andolfi, L., Canters, G.W., Verbeet, M.P., Cannistraro, S., 2004b. Scanning tunneling spectroscopy investigation of self-assembled plastocyanin mutants onto gold substrates under controlled environment. *Biophys. Chem.* **107**, 107–116.

Anschutz, A.J., Penn, R.L., 2005. Reduction of crystalline iron(III) oxyhydroxides using hydroquinone: Influence of phase and particle size. *Geochem. Trans.* **6**, 60–66.

Avouris, P., Lyo, I.W., Molinasmata, P., 1995. STM studies of the interaction of surface-state electrons on metals with steps and adsorbates. *Chem. Phys. Lett.* **240**, 423–428.

Becker, U., Hochella, M.F., Apra, E., 1996. The electronic structure of hematite{001} surfaces: applications to the interpretation of STM images and heterogeneous surface reactions. *Am. Mineral.* **81**, 1301–1314.

Beliaev, A.S., Saffarini, D.A., Mclaughlin, J.L., Hunnicutt, D., 2001. MtrC, an outer membrane decahaem *c* cytochrome required for metal reduction in *Shewanella putrefaciens* MR-1. *Mol. Microbiol.* **39**, 722–730.

Bonanni, B., Alliata, D., Bizzarri, A.R., Cannistraro, S., 2003. Topological and electron-transfer properties of yeast cytochrome *c* adsorbed on bare gold electrodes. *Chemphyschem* **4**, 1183–1188.

Boussaad, S., Tao, N.J., 1999. Electron transfer and adsorption of myoglobin on self-assembled surfactant films: an electrochemical tapping-mode AFM study. *J. Am. Chem. Soc.* **121**, 4510–4515.

Chi, Q.J., Zhang, J.D., Nielsen, J.U., Friis, E.P., Chorkendorff, I., Canters, G.W., Andersen, J.E.T., Ulstrup, J., 2000. Molecular monolayers and interfacial electron transfer of Pseudomonas aeruginosa azurin on Au(111). *J. Am. Chem. Soc.* **122**, 4047–4055.

Chi, Q.J., Zhang, J.D., Andersen, J.E.T., Ulstrup, J., 2001. Ordered assembly and controlled electron transfer of the blue copper protein azurin at gold (111) single-crystal substrates. *J. Phys. Chem. B* **105**, 4669–4679.

Davis, J.J., Djuricic, D., Lo, K.K.W., Wallace, E.N.K., Wong, L.L., Hill, H.A.O., 2000. A scanning tunneling study of immobilised cytochrome $P450_{cam}$. *Faraday Discuss.* **116**, 15–22.

Davis, J.J., Hill, H.A.O., 2002. The scanning probe microscopy of metalloproteins and metalloenzymes. *Chem. Commun.*, 393–401.

Davis, J.J., Wrathmell, C.L., Zhao, J., Fletcher, J., 2004. The tunnelling conductance of molecularly ordered metalloprotein arrays. *J. Mol. Recognit.* **17**, 167–173.

Davis, J.J., Morgan, D.A., Wrathmell, C.L., Axford, D.N., Zhao, J., Wang, N., 2005. Molecular bioelectronics. *J. Mater. Chem.* **15**, 2160–2174.

Davis, L.C., Everson, M.P., Jaklevic, R.C., Shen, W.D., 1991. Theory of the local density of surface-states on a metal—comparison with scanning tunneling spectroscopy of a Au(111) surface. *Phys. Rev. B* **43**, 3821–3830.

Dichristina, T.J., Fredrickson, J.K., Zachara, J.M., 2005. Enzymology of electron transport: energy generation with geochemical consequences. In: Banfield, J.F., Cervini-Silva, J., Nealson, K.H. (Eds.), *Molecular Geomicrobiology*, vol. 59. Mineralogical Society of America, pp. 27–52.

Duwez, A.S., 2004. Exploiting electron spectroscopies to probe the structure and organization of self-assembled monolayers: a review. *J. Electron Spectrosc.* **134**, 97–138.

Eggleston, C.M., Khare, N., Lovelace, D.M., 2006. Cytochrome *c* interaction with hematite (α-Fe_2O_3) surfaces. *J. Electron Spectrosc.* **150**, 220–227.

Friis, E.P., Andersen, J.E.T., Kharkats, Y.I., Kuznetsov, A.M., Nichols, R.J., Zhang, J.D., Ulstrup, J., 1999. An approach to long-range electron transfer mechanisms in metalloproteins: in situ scanning tunneling microscopy with submolecular resolution. *Proc. Natl. Acad. Sci. USA* **96**, 1379–1384.

Gilbert, B., Banfield, J.F., 2005. Molecular-scale processes involving nanoparticulate minerals in biogeochemical systems. In: Banfield, J.F., Cervini-Silva, J., Nealson, K.H. (Eds.), *Molecular Geomicrobiology*, vol. 59. Mineralogical Society of America, pp. 109–155.

Gorby, Y.A., Yanina, S., Mclean, J.S., Rosso, K.M., Moyles, D., Donhalkova, A., Beveridge, T.J., Chang, I.S., Kim, B.H., Culley, D.E., Reed, S.B., Romine, M.F., Saffarini, D.A., Hill, E.A., Shi, L., Elias, D.A., Kennedy, D.W., Pinchuk, G., Wantanabe, K., Ishii, S., Logan, B., Nealson, K.H., Fredrickson, J.K., 2006. Electrically conductive bacterial nanowires produced by *Shewanella oneidensis* MR-1 and other microorganisms. *Proc. Natl. Acad. Sci. USA* **103**, 11358–11363.

Gray, H.B., Winkler, J.R., 2003. Heme protein dynamics: electron tunneling and redox triggered folding. In: Kadish, K.M., Smith, K.M., Guilard, R. (Eds.), *The Porphyrin Handbook*, *Bioinorganic and Bioorganic Chemistry*, vol. 11. Academic Press, pp. 51–73.

Hamers, R.J., 1993. Methods of tunneling spectroscopy with STM. In: Bonnell, D.A. (Ed.), *Scanning Tunneling Microscopy and Spectroscopy: Theory, Techniques, and Applications*. John Wiley and Sons, pp. 51–189.

Han, W.H., Durantini, E.N., Moore, T.A., Moore, A.L., Gust, D., Rez, P., Leatherman, G., Seely, G.R., Tao, N.J., Lindsay, S.M., 1997. STM contrast, electron-transfer chemistry, and conduction in molecules. *J. Phys. Chem. B* **101**, 10719–10725.

Hansen, A.G., Boisen, A., Nielsen, J.U., Wackerbarth, H., Chorkendorff, I., Andersen, J.E.T., Zhang, J.D., Ulstrup, J., 2003. Adsorption and interfacial electron transfer of Saccharomyces cerevisiae yeast cytochrome *c* monolayers on Au(111) electrodes. *Langmuir* **19**, 3419–3427.

Hochella, M.F., 2002. Nanoscience and technology: the next revolution in the Earth sciences. *Earth Planet. Sci. Lett.* **203**, 593–605.

Kappler, A., Straub, K.L., 2005. Geomicrobiological cycling of iron. In: Banfield, J.F., Cervini-Silva, J., Nealson, K.H. (Eds.), *Molecular Geomicrobiology*, vol. 59. Mineralogical Society of America, pp. 85–108.

Kerisit, S., Rosso, K.M., 2006. Computer simulation of charge transfer at hematite surfaces. *Geochim. Cosmochim. Acta* **70**, 1888–1903.

Khare, N., Eggleston, C.M., Lovelace, D.M., 2005. Sorption and direct electrochemistry of mitochondrial cytochrome *c* on hematite surfaces. *Clay Clay Miner.* **53**, 564–571.

Kowalczyk, P., Kozlowski, W., Olejniczak, W., Datta, P.K., 2006. STS investigations of temperature dependence of Au(111) surface state energy position. *Surf. Sci.* **600**, 1604–1607.

Kuznetsov, A.M., Sommerlarsen, P., Ulstrup, J., 1992. Resonance and environmental fluctuation effects in STM currents through large adsorbed molecules. *Surf. Sci.* **275**, 52–64.

Lies, D.P., Hernandez, M.E., Kappler, A., Mielke, R.E., Gralnick, J.A., Newman, D.K., 2005. *Shewanella oneidensis* MR-1 uses overlapping pathways for iron reduction at a distance and by direct contact under conditions relevant for biofilms. *Appl. Environ. Microbiol.* **71**, 4414–4426.

Lindsay, S.M., 1993. Biological applications of the scanning probe microscope. In: Bonnell, D.A. (Ed.), *Scanning Tuennling Microscopy and Spectroscopy: Theory, Techniques, And Applications*. John Wiley and Sons, pp. 335–408.

Lo, K.K.W., Wong, L.L., Hill, A.O., 1999. Surface-modified mutants of cytochrome P450(cam): enzymatic properties and electrochemistry. *FEBS Lett.* **451**, 342–346.

Lovley, D.R., Holmes, D.E., Nevin, K.P., 2004. Dissimilatory Fe(III) and Mn(IV) reduction. *Adv. Microb. Physiol.* **49**, 219–286.

Lower, B.H., Hochella Jr., M.F., Lower, S.K., 2005. Putative mineral-specific proteins synthesized by a metal reducing bacterium. *Am. J. Sci.* **305**, 687–710.

Lower, S.K., Hochella, M.F.J., Beveridge, T.J., 2001. Bacterial recognition of mineral surfaces: nanoscale interactions between Shewanella and α-FeOOH. *Science* **292**, 1360–1363.

Marcus, R.A., Sutin, N., 1985. Electron transfers in chemistry and biology. *Biochim. Biophys. Acta* **811**, 265–322.

McCreery, R.L., 2004. Molecular electronic junctions. *Chem. Mater.* **16**, 4477–4496.

Morimoto, J., Tanaka, H., Kawai, T., 2005. Direct measurement of electron transport features in cytochrome *c* via V-I characteristics of STM currents. *Surf. Sci.* **580**, L103–L108.

Myers, C.R., Nealson, K.H., 1988. Bacterial manganese reduction and growth with manganese oxide as the sole electron acceptor. *Science* **240**, 1319–1321.

Myers, C.R., Myers, J.M., 1997. Outer membrane cytochromes of *Shewanella putrefaciens* MR-1: Spectral analysis, and purification of the 83-kDa *c*-type cytochrome. *Biochim. Biophys. Acta, Biomembranes* **1326**, 307–318.

Myers, C.R., Myers, J.M., 2004. The outer membrane cytochromes of *Shewanella oneidensis* MR-1 are lipoproteins. *Lett. Appl. Microbiol.* **39**, 466–470.

Myers, J.M., Myers, C.R., 1998. Isolation and sequence of omcA, a gene encoding a decaheme outer membrane cytochrome *c* of *Shewanella putrefaciens* MR-1, and detection of omcA homologs in other strains of *S. putrefaciens*. *Biochim. Biophys. Acta* **1373**, 237–251.

Myers, J.M., Myers, C.R., 2003. Overlapping role of the outer membrane cytochromes of *Shewanella oneidensis* MR-1 in the reduction of manganese(IV) oxide. *Lett. Appl. Microbiol.* **37**, 21–25.

Neal, A.L., Rosso, K.M., Geesey, G.G., Gorby, Y.A., Little, B.J., 2003. Surface structure effects on direct reduction of iron oxides by *Shewanella oneidensis*. *Geochim. Cosmochim. Acta* **67**, 4489–4503.

Neal, A.L., Bank, T.L., Hochella, M.F.J., Rosso, K.M., 2005. Cell adhesion of *Shewanella oneidensis* to iron oxide minerals: effect of different single crystal faces. *Geochem. Trans.* **6**, 77–84.

Nealson, K.H., Stahl, D.A., 1997. Microorganisms and biogeochemical cycles: what can we learn from layered microbial communities? In: Banfield, J.F., Nealson, K.H. (Eds.), *Geomicrobiology: Interactions between Microbes and Minerals*, vol. 35. Mineralogical Society of America, pp. 5–34.

Nealson, K.H., Belz, A., Mckee, B., 2002. Breathing metals as a way of life: geobiology in action. *Antonie van Leeuwenhoek* **81**, 215–222.

Newman, D.K., Kolter, R., 2000. A role for excreted quinones in extracellular electron transfer. *Nature* **405**, 94–97.

Newman, D.K., Banfield, J.F., 2002. Geomicrobiology: how molecular-scale interactions underpin biogeochemical systems. *Science* **296**, 1071–1077.

Nitzan, A., Ratner, M.A., 2003. Electron transport in molecular wire junctions. *Science* **300**, 1384–1389.

Page, C.C., Moser, C.C., Chen, X.X., Dutton, P.L., 1999. Natural engineering principles of electron tunnelling in biological oxidation-reduction. *Nature* **402**, 47–52.

Patel, N., Davies, M.C., Lomas, M., Roberts, C.J., Tendler, S.J.B., Williams, P.M., 1997. STM of insulators with the probe in contact with an aqueous layer. *J. Phys. Chem. B* **101**, 5138–5142.

Pitts, K.E., Dobbin, P.S., Reyes-Ramirez, F., Thomson, A.J., Richardson, D.J., Seward, H.E., 2003. Characterization of the *Shewanella oneidensis* MR-1 decaheme cytochrome MtrA. *J. Biol. Chem.* **278**, 27758–27765.

Poirier, G.E., 1997. Characterization of organosulfur molecular monolayers on Au(111) using scanning tunneling microscopy. *Chem. Rev.* **97**, 1117–1127.

Pomerantz, M., Aviram, A., Mccorkle, R.A., Li, L., Schrott, A.G., 1992. Rectification of STM current to graphite covered with phthalocyanine molecules. *Science* **255**, 1115–1118.

Reguera, G., Mccarthy, K.D., Mehta, T., Nicoll, J.S., Tuominen, M.T., Lovley, D.R., 2005. Extracellular electron transfer via microbial nanowires. *Nature* **435**, 1098–1101.

Rosso, K.M., Zachara, J.M., Fredrickson, J.K., Gorby, Y.A., Smith, S.C., 2003. Nonlocal bacterial electron transfer to hematite surfaces. *Geochim. Cosmochim. Acta* **67**, 1081–1087.

Ruebush, S.S., Icopini, G.A., Brantley, S.L., Tien, M., 2006. In vitro enzymatic reduction kinetics of mineral oxides by membrane fractions from *Shewanella oneidensis* MR-1. *Geochim. Cosmochim. Acta* **70**, 56–70.

Savitzky, A., Golay, M.J.E., 1964. Smoothing and differentiation of data by simplified least squares procedures. *Anal. Chem.* **36**, 1627–1638.

Schmickler, W., 1993. Investigation of electrochemical electron-transfer reactions with a scanning tunneling microscope—a theoretical study. *Surf. Sci.* **295**, 43–56.

Schoenfisch, M.H., Pemberton, J.E., 1998. Air stability of alkanethiol self-assembled monolayers on silver and gold surfaces. *J. Am. Chem. Soc.* **120**, 4502–4513.

Schroder, I., Johnson, E., De Vries, S., 2003. Microbial ferric iron reductases. *FEMS Microbiol. Rev.* **27**, 427–447.

Shi, L., Lin, J.T., Markillie, L.M., Squier, T.C., Hooker, B.S., 2005. Overexpression of multiheme *c*-type cytochromes. *BioTechniques* **38**, 297–299.

Shi, L., Chen, B., Wang, Z., Elias, D.A., Mayer, U., Gorby, Y.A., Ni, S., Lower, B.H., Kennedy, D.W., Wunschel, D.S., Mottaz, H.M., Marshall, M.J., Hill, E.A., Beliaev, A.S., Zachara, J.M., Fredrickson, J.K., Squier, T.C., 2006. Isolation of high-affinity functional protein complex between OmcA and MtrC: two outer membrane decaheme *c*-

type cytochromes of *Shewanella oneidensis* MR-1. *J. Bacteriol.* **188**, 4705–4714.

Simonson, T., 2003. Electrostatics and dynamics of proteins. *Rep. Prog. Phys.* **66**, 737–787.

Stack, A.G., Rosso, K.M., Smith, D.M.A., Eggleston, C.M., 2004. Reaction of hydroquinone with hematite II. Calculated electron-transfer rates and comparison to the reductive dissolution rate. *J. Colloid Interface Sci.* **274**, 442–450.

Stamouli, A., Frenken, J.W.M., Oosterkamp, T.H., Cogdell, R.J., Aartsma, T.J., 2004. The electron conduction of photosynthetic protein complexes embedded in a membrane. *FEBS Lett.* **560**, 109–114.

Tao, N.J., 1996. Probing potential-tuned resonant tunneling through redox molecules with scanning tunneling microscopy. *Phys. Rev. Lett.* **76**, 4066–4069.

Tersoff, J., Hamann, D.R., 1985. Theory of the scanning tunneling microscope. *Phys. Rev. B* **31**, 805–813.

Tiedje, J.M., 2002. Shewanella—the environmentally versatile genome. *Nat. Biotechnol.* **20**, 1093–1094.

Uchimiya, M., Stone, A.T., 2006. Redox reactions between iron and quinones: thermodynamic contraints. *Geochim. Cosmochim. Acta* **70**, 1388–1401.

Vargas, M., Kashefi, K., Blunt-Harris, E.L., Lovley, D.R., 1998. Microbiological evidence for Fe(III) reduction on early Earth. *Nature* **395**, 65–67.

Venkateswaran, K., Moser, D.P., Dollhopf, M.E., Lies, D.P., Saffarini, D.A., Macgregor, B.J., Ringelberg, D.B., White, D.C., Nishijima, M., Sano, H., Burghardt, J., Stackebrandt, E., Nealson, K.H., 1999. Polyphasic taxonomy of the genus Shewanella and description of *Shewanella oneidensis* sp. nov. *Int. J. Syst. Bacteriol.* **49**, 705–724.

Vericat, C., Vela, M.E., Salvarezza, R.C., 2005. Self-assembled monolayers of alkanethiols on Au(111): surface structures, defects and dynamics. *Phys. Chem. Chem. Phys.* **7**, 3258–3268.

Vondrak, T., Cramer, C.J., Zhu, X.Y., 1999. The nature of electronic contact in self-assembled monolayers for molecular electronics: evidence for strong coupling. *J. Phys. Chem. B* **103**, 8915–8919.

Yang, G.H., Liu, G.Y., 2003. New insights for self-assembled monolayers of organothiols on Au(111) revealed by scanning tunneling microscopy. *J. Phys. Chem. B* **107**, 8746–8759.

Zhang, J., Chi, Q., Kuznetsov, A.M., Hansen, A.G., Wackerbarth, H., Christensen, H.E.M., Andersen, J.E.T., Ulstrup, J., 2002. Electronic properties of functional biomolecules at metal/aqueous solution interfaces. *J. Phys. Chem. B* **106**, 1131–1152.

Zhang, J.D., Kuznetsov, A.M., Ulstrup, J., 2003a. In situ scanning tunnelling microscopy of redox molecules. Coherent electron transfer at large bias voltages. *J. Electroanal. Chem.* **541**, 133–146.

Zhang, J.D., Welinder, A.C., Hansen, A.G., Christensen, H.E.M., Ulstrup, J., 2003b. Catalytic monolayer voltammetry and in situ scanning tunneling microscopy of copper nitrite reductase on cysteamine-modified Au(111) electrodes. *J. Phys. Chem. B* **107**, 12480–12484.

Zhang, J.D., Christensen, H.E.M., Ooi, B.L., Ulstrup, J., 2004. In situ STM imaging and direct electrochemistry of Pyrococcus furiosus ferredoxin assembled on thiolate-modified Au(111) surfaces. *Langmuir* **20**, 10200–10207.